POLITECNICO DI TORINO
Repository ISTITUZIONALE

Thermally triggered nanorocket from double-walled carbon nanotube in water

(Article begins on next page)

01 September 2025

Thermally triggered nanorocket from double-walled carbon nanotube in water

Matteo Fasano[a], Alessandro Crisafulli[a], Annalisa Cardellini[a], Luca Bergamasco[a], Eliodoro Chiavazzo[a] and Pietro Asinari[a]

[a]Department of Energy - Politecnico di Torino, Corso Duca degli Abruzzi 24, 10129 Torino (Italy)

ABSTRACT
In this work, we propose and investigate the use of double-walled carbon nanotubes (DWCNTs) as nanosized rockets. The nanotubes are immersed in water, and the propulsion of inner nanotube is achieved by heating the water encapsulated within the DWCNT. Considering a setup made of (5,5)(8,8) DWCNT, molecular dynamics simulations for different water temperatures show that the trajectory can be divided into four phases: trigger, expulsion, damping and final equilibrium. After analysing the dynamics and the involved forces, we find out that the inner nanotube expulsion is mainly controlled by van der Waals interactions between the nanotubes; whereas, the damping role is predominantly played by the external aqueous environment. Based on these results, we propose an analytical model able to predict both the triggering time for a given water temperature and the whole dynamics of nanorocket. The validity of such dynamical model can be extended also to a broader variety of DWCNT configurations, once the different forces acting on the inner nanotube are provided. The proposed model may contribute to assist the design of nanorockets in several nanotechnology applications, such as triggered drug delivery, cell membrane piercing, or colloids with thermophoretic properties.

1. Introduction

Energy conversion into nanoscale motion is one of the most fervid and fascinating topics of current nanotechnology research. Most of the hectic scientific activity in this framework owes to the potential applications of the so-called *nanomotors*, which span over a wide range of technological, environmental and biomedical problems, such as drug delivery, hazardous monitoring, controlled nano-functionalization and micro-manipulation [1–4]. In this view, many efforts have been spent during the last decades on the development of artificial nanomotors - eventually mimicking Nature [5] - with particular emphasis on motion control [6] and propulsion, e.g. for micro and nanoscale rockets and shuttles [7,8].

The use of carbon nanotubes (CNTs) as nanomotors has been extensively investigated. In an eminent and pioneering work, Cumings *et al.* demonstrated the con-

---

Corresponding author: P. Asinari. Email: pietro.asinari@polito.it

trolled and reversible telescopic extensibility potential of multi-walled carbon nanotubes (MWCNTs), which makes them suitable for ultralow-friction nanoscale linear bearings and constant-force nanosprings [9]. This work stimulated further ideas and analysis of other possible applications, such as gigahertz oscillators [10,11], linear servomotors [12], and similar solutions employing single-walled [13] or double-walled CNTs [14,15]. Molecular dynamics (MD) simulations have been employed to get more insight into the behaviour of thermally-driven nanomotors based on MWCNTs, for instance to investigate how size and chirality of nanotubes determine their motion [16–18]. Kang *et al.* studied a MWCNT oscillator controlled by thermal gas expansion and found that - for sufficiently high temperatures - the retention force due to van der Waals interactions is lower than the pull-out force due to gas-expansion and, thus, the inner nanotube can be ejected [19]. Other studies demonstrated that this pull-out force is 3-4 times higher in nanotubes with broken ends rather than capped ones [20], and that it scales with the diameter of the outer nanotube at the sliding interface [21–23].

In this work, we propose the use of solvated double-walled carbon nanotubes (DWCNTs) as thermally-triggered nanorockets. The nanotubes are immersed in water, and the propulsion of the inner nanotube is provided by heating water molecules in the enclosed volume within the DWCNT. Molecular dynamics simulations are performed considering a setup made of (5,5)(8,8) DWCNT at different temperatures of encapsulated water, showing that the heating temperature does not sensibly affect nanorocket dynamics but only triggering time. Moreover, the analysis of simulation trajectories shows that the inner nanotube motion can be divided into four stages: trigger, expulsion, damping and final equilibrium. After having investigated these stages and the related forces, we propose an analytical model predicting the nanorocket dynamics. A comparison of the proposed model with simulation data shows excellent agreement also in case of different DWCNT sizes, suggesting possible guidelines to the actual use of MWCNT-based rockets in biomedical and engineering applications.

2. Methods

The dynamics of the DWCNT-based nanorocket is investigated by MD simulations using the open-source GROMACS package [24]. Figure 1(a) shows the considered (5,5)/(8,8) DWCNT, which presents two capped ends on the left side and two open ends on the right side. The capped ends of the inner and outer nanotube encapsulate water molecules (red and white atoms in Fig. 1(a)) [25], and the whole system is completely immersed in water (not represented in Fig. 1(a) for clarity). Instead, Fig. 1(b) specifies the geometrical characteristics of the initial configuration: the inner (D) and outer (D') diameters are equal to 0.67 nm and 1.09 nm, respectively; the lengths of nanotubes, L and L', are respectively 4.02 nm and 8.34 nm; finally, Δ, namely the distance between the open ends of nanotubes, is equal to 0.32 nm. Bonded interactions between carbon atoms are modelled by stretch, angle and dihedral harmonic potentials, whose parameters are reported elsewhere [26]. On the other hand, 12-6 Lennard-Jones potential is employed for van der Waals interactions:

$$V_{LJ} = 4\varepsilon \left[\left(\frac{\sigma}{r} \right)^{12} - \left(\frac{\sigma}{r} \right)^{6} \right], \tag{1}$$

where r is the distance between two atoms, ε and σ are the potential well and the van der Waals radius, respectively [26,27]. Lorentz-Berthelot combination rules are considered

for modelling van der Waals interactions between the nanotubes and water. The cut-off distance of non-bonded interactions is set to $1.2\,\text{nm}$.
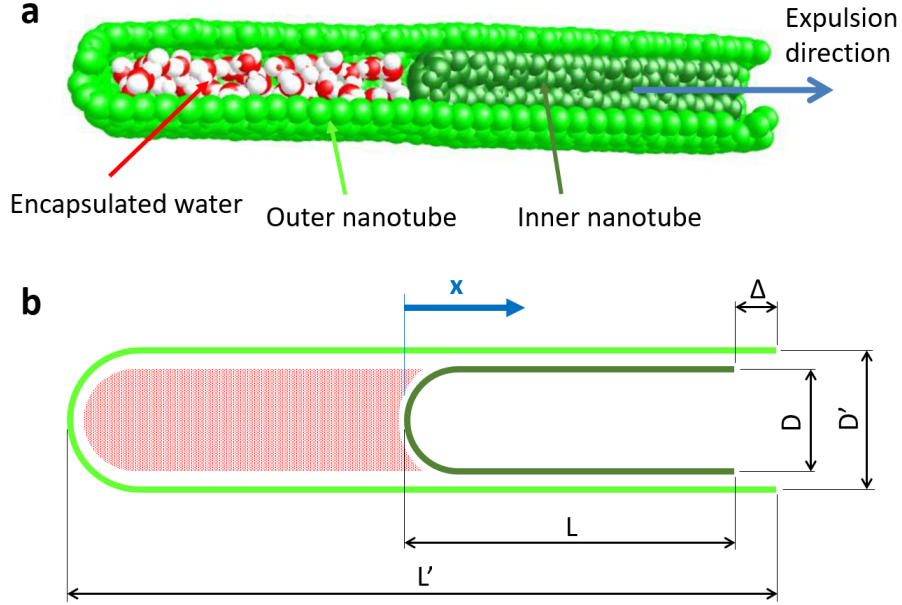

Figure 1. Nanorocket configuration. (a) Section of the outer nanotube (light green) and inner nanotube (dark green) with encapsulated water inside the hollow space (white and red). The direction of inner nanotube expulsion is indicated by the blue arrow. Note that the double-walled nanotube is completely immersed in a water box, which is not represented here for clarity. (b) Scheme of the geometrical configuration of the simulated DWCNT with relative dimensions and reference system.

The capped nanotubes are generated through the NanoCap routine [28]; after that, the double-walled configuration is assembled by translating the smaller nanotube into the larger one. The initial geometry does not contain water molecules, and it is first energy minimized to avoid possible bad contacts between the nanotubes. The simulation box ($25\text{x}7\text{x}7$ nm^3) is then solvated by SPC/E water molecules [29] with a target water density equal to 997 g/cm^3 in the bulk region (300 K, 1 bar), and energy minimisation performed again. The configuration is subsequently equilibrated following two consecutive steps. In a first step, the system is simulated in the NVT ensemble for 100 ps, using Nosé-Hoover thermostat (300 K) [30]. In a second step, the system is equilibrated in the NPT ensemble for 100 ps, employing Nosé-Hoover thermostat (300 K) and isotropic Parrinello-Rahman barostat (1 bar) [31].

After system equilibration, the expulsion of the inner nanotube is triggered by heating up the encapsulated water molecules (either 25 or 30 in the (5,5)(8,8) configuration) by a Nosé-Hoover thermostat at T_{heat} temperature. This thermostat is applied - during the whole simulation - to the initially encapsulated water molecules. Note that this condition could be experimentally implemented by encapsulating also plasmonic or superparamagnetic nanoparticles within the DWCNT, since they could be heated up by either near-infrared laser or alternating magnetic field [32,33]. Specifically, different T_{heat} are tested, ranging from 1000 K to 2200 K with steps of 200 K. Such localised temperature increase has been predicted and experimentally measured, for instance, in case of plasmonic nanoparticles or nanodots irradiated by laser sources [34–38]. Instead, water molecules outside the DWCNT (*i.e.* the total number of water molecules in the box

3

reduced by the number of encapsulated water molecules, namely 40190 in the (5,5)(8,8) configuration) are not coupled to a thermostat and, thus, their temperature can freely evolve. During all nanorocket dynamics, a isotropic Parrinello-Rahman barostat at 1 bar is coupled to the simulation box to avoid pressure build up, and energy conservation is verified throughout the different dynamical phases per each considered setup. Seven repetitions are carried out per each simulated T_{heat}, and results are reported in terms of average values and their standard deviation.

To ease the measure of system dynamics during the production run, one carbon ring of the external nanotube far from the inner nanotube is fixed by harmonic restraints along x direction (*i.e.* the direction of inner nanotube motion), taking a spring constant equal to 10000 kJ mol^{-1} nm^{-2}. All molecular dynamics runs are carried out using a leap-frog algorithm [39], considering the same 1 fs time step for all bonded and non-bonded interactions. Notice that more efficient multiple-time-stepping algorithms may be used to improve the computational performance of the integrator [40]. Bonded interactions within the SPC/E water model are treated using the SETTLE algorithm [41]. Periodic boundary conditions along x, y, and z Cartesian axes are considered in all simulations. Time constants of Nosé-Hoover thermostat and isotropic Parrinello-Rahman barostat are equal to 0.2 ps and 2.0 ps, respectively; whereas, water compressibility is taken as $4.5 \cdot 10^{-5}$ bar^{-1}.

3. Results

Figure 2 shows the dynamics of inner nanotube expulsion in the case of $T_{heat} = 1600$ K, namely the position (x), velocity ($\dot{x}$) and acceleration ($\ddot{x}$) of its centre of mass. Note that these quantities are computed in relative terms, where the reference is considered as the centre of mass of the outer nanotube (see Fig. 1(a)). Focusing on the velocity trend, four different phases of motion can be distinguished. In the first phase (0 ps $< t <$ 10.4 ps), the velocity of the inner nanotube is approximately null. In the second phase (10.4 ps $< t <$ 13.8 ps), the velocity rapidly increases until it reaches a maximum. After that, the velocity of the inner nanotube gradually decreases (third phase) and it eventually plateaus to zero (fourth phase), when the expulsion transient is completed. Analogously, four distinct phases can be identified for both relative position and resulting acceleration between the two nanotubes. Specifically, after the first 10.4 ps, the inner nanotube undergoes a strong acceleration, which suddenly drops after $t = 13.8$ ps.

Figure 3 reports the duration of these phases as a function of the temperature of encapsulated water (T_{heat}). In particular, Fig. 3(b) highlights that the duration of second and third phase is not significantly affected by T_{heat}. Conversely, the time window preceding the expulsion of the inner CNT is clearly determined by the temperature of encapsulated water (see Fig. 3(a)). The instant of inner nanotube expulsion (t_e), which corresponds to the duration of the first phase, is observed to reduce with T_{heat} following an Arrhenius-like law:

$$t_e = k_1 \cdot \exp\left(\frac{k_2}{T_{heat}}\right), \tag{2}$$

where k_1 and k_2 can be calculated by fitting simulation results. Note that, according to Arrhenius model, k_2 should depend on the Boltzmann constant (k_B) and the activation energy of the phenomenon (E_a) as $k_2 = E_a/k_B$; whereas, k_1 should be considered as
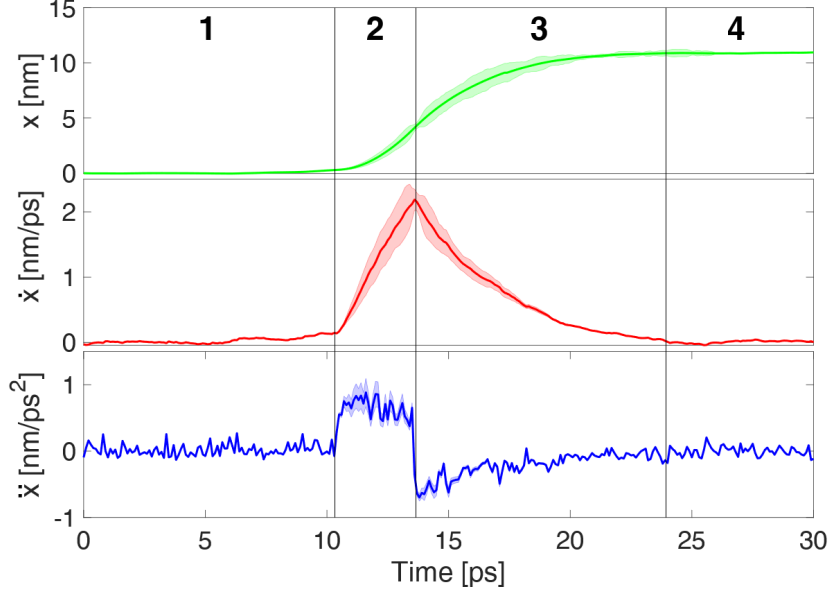
4

Figure 2. Simulated dynamics of the inner nanotube, for encapsulated water temperature $T_{heat} = 1600\,$K. During the first phase (labelled with **1**), which extends up to $t = 10.4\,$ps, the motion of the nanotube is negligible. In the second phase (**2**), the nanotube motion is characterised by a uniform acceleration; hence, the velocity linearly increases until exceeding $2\,$nm/ps at $t = 13.8\,$ps. In the third phase (**3**), the acceleration drops to negative values and then gradually goes to zero. After $24\,$ps, in the fourth phase (**4**), the nanotube reaches its final equilibrium condition. The shaded areas represent standard deviation of the reported average quantities after that the inner nanotube motion has been triggered (from phase 2 onwards), computed over seven independent repetitions.

the inverse of the frequency factor (A), namely $k_1 = 1/A$. The solid lines in Fig. 3(a) show Eq. 2 best fitted to the MD results obtained in case of 30 or 25 water molecules encapsulated between the CNT caps. By considering the same activation energy while different frequency factors, Eq. 2 is best fitted ($R^2 > 0.95$) to simulation results if $k_2 = 3557\,$K and $k_1 = 2.22\,$ps (30 water molecules) or $k_1 = 4.90\,$ps (25 water molecules). Hence, coherently with Arrhenius law, the frequency factor scales with the number of inter-molecular collisions, which is proportional to the number of encapsulated water molecules.

More insights on the nanorocket dynamics can be obtained by the time evolution of non-bonded (van der Waals) interactions between inner and outer nanotube, as reported in Fig. 4. During the first $10.4\,$ps, a reciprocal repulsion between the nanotubes is evident, therefore highlighting metastable equilibrium conditions for the initial (5,5)(8,8) DWCNT configuration [42]. Successively, when the inner nanotube expulsion begins, the repulsive potential linearly decreases with the reduced contact area between the CNTs. At the end of the second phase, namely at $t = 13.8\,$ps, the non-bonded interaction energy between CNTs eventually vanishes. Clearly, the trend of van der Waals interactions is strictly related to the DWCNT configuration and geometry [42]; therefore, it should be re-evaluated in case of different nanorocket designs.
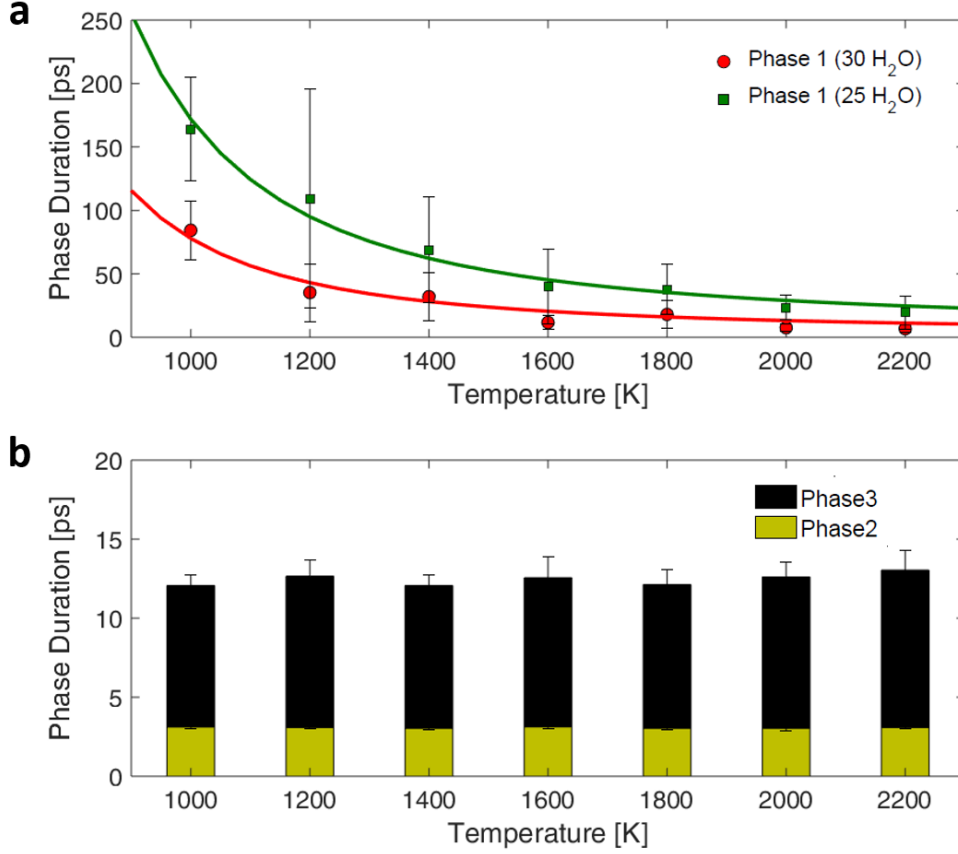
Figure 3. Average duration of the phases during the inner CNT motion, as a function of the encapsulated water temperature (T_{heat}). (a) Average duration of the first phase. Symbols refer to MD data, while solid red and green lines describe the trend of the proposed fitting equation (Eq. 2) for 30 and 25 molecules of encapsulated water. (b) Average duration of phases 2 (yellow) and 3 (black) and their respective standard deviation at different temperatures.

4. Discussion

In the considered DWCNT-based nanorocket, the dynamics of inner nanotube expulsion is first characterised by the trigger phase, which is mainly governed by the pressure force exerted by encapsulated water molecules; then, the expulsion, damping and equilibrium phases follow, which are determined by a balance between van der Waals, inertial and viscous forces acting on the inner nanotube. As a representative case for the setup made of (5,5)(8,8) DWCNT, here we analyse the nanorocket dynamics for $T_{heat} = 1600$ K. Nevertheless, as already pointed out, the temperature of encapsulated water does not significantly affect the nanorocket dynamics after the trigger phase and, therefore, similar considerations can be extended to all the considered simulations with the (5,5)(8,8) DWCNT setup.

The temperature transient of encapsulated water, and thus the triggering time of inner nanotube expulsion, is found to last few picoseconds due to the limited amount of encapsulated water molecules. However, the triggering time of inner nanotube expulsion may be longer in experimental implementations of the nanorocket, since the temperature increase in the encapsulated region would be slowed down by the thermal diffusion
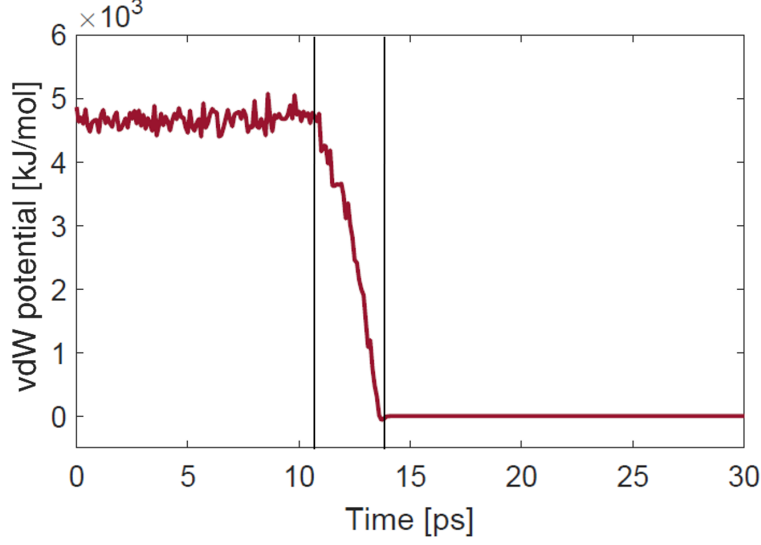
6

Figure 4. Van der Waals potential between inner and outer CNT during a simulation at $T_{heat} = 1600\,\mathrm{K}$. When $t < 10.4\,\mathrm{ps}$, van der Waals potential is constant and fluctuating around a positive value. During the second phase ($10.4\,\mathrm{ps} < t < 13.8\,\mathrm{ps}$), interaction energy decreases linearly. When the expulsion of the inner CNT is completed, van der Waals potential drops to zero.

mechanism from heated nanoparticles to encapsulated water (indicatively, in the range of few tens or hundreds of picoseconds, according to the nanoparticle size [43,44]).

In the trigger phase (phase 1), encapsulated and external water molecules hit the inner nanotube in opposite directions, therefore causing competing pressure forces on the nanotube (F_i and F_e in Fig. 5, respectively). Since encapsulated water has a temperature ($T_{heat} = 1600\,\mathrm{K}$) significantly higher than the external one ($T \cong 300\,\mathrm{K}$), $F_i \gg F_e$ and, after a time interval dependent on T_{heat} according to Eq. 2, this triggers the inner nanotube expulsion. Although the low number of water molecules in the encapsulated volume leads to large oscillations in the F_i value (red line in Fig. 5(b)), the average internal force exerted by 30 water molecules on the inner nanotube during phase 1 is equal to 0.173 nN.

As evident from Fig. 5(b), F_i plays a role only in the first phase and then it decays to zero after $t = 10.4\,\mathrm{ps}$, when a slight variation of the relative position between inner and outer nanotubes triggers the expulsion phase (phase 2). During this phase, two main contributions dominate the inner nanotube dynamics: the non-bonded interactions between inner and outer nanotubes (F_{vdW} in Fig. 5) and the viscous damping given by external water (F_v in Fig. 5). In fact, the progressive decrease of van der Waals interactions between the CNTs (see Fig. 4) induces the expulsion force F_{vdW} on the inner nanotube, whose motion is naturally damped by external water viscosity. Considering only phase 2, the simulated values of F_{vdW} in Fig. 5(b) can be interpolated by a piecewise-defined function, namely:

$$
F_{vdW} = \begin{cases}
a \cdot t + b, & \text{if } 10.4\,\mathrm{ps} < t \leq 10.85\,\mathrm{ps} \\
d \cdot t + e, & \text{if } 10.85\,\mathrm{ps} < t \leq 13.55\,\mathrm{ps} \\
f \cdot t + g, & \text{if } 13.55\,\mathrm{ps} < t \leq 13.8\,\mathrm{ps}
\end{cases} \tag{3}
$$

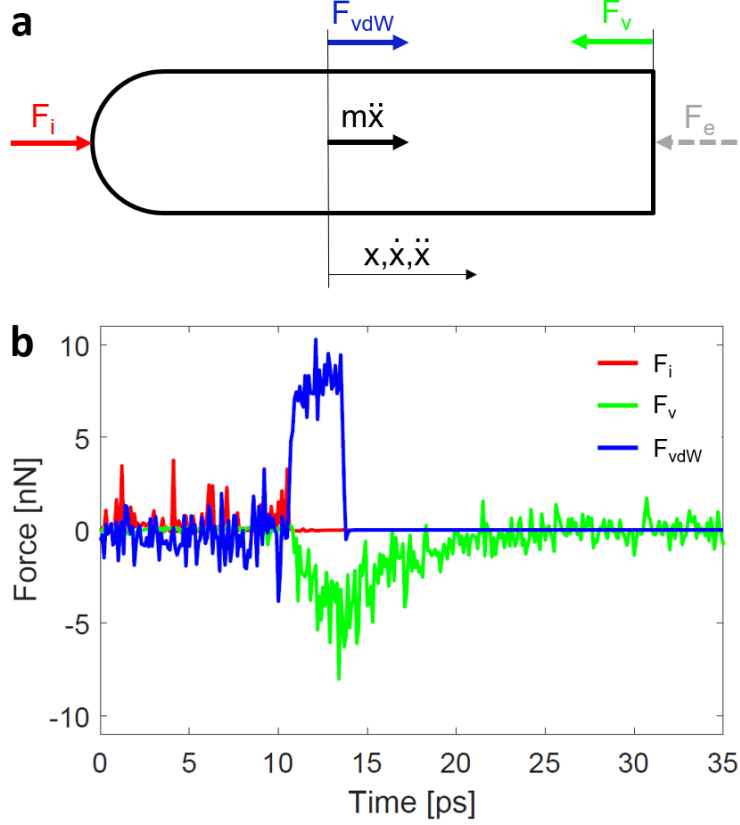with values of fitting coefficients reported in Tab. 1.

7

Figure 5. Balance of forces acting on the inner CNT for $T_{heat} = 1600\,\mathrm{K}$. (a) Free body diagram of the inner CNT. Note that the force due to the external water pressure (F_e) here shows negligible values respect to the other contributions. Forces are considered as positive if concordant with the expulsion direction. (b) Trend of the forces acting on the inner CNT during the first 35 ps of simulation. The force due to encapsulated water pressure (F_i) and the viscous forces exerted by the external water on the nanotube (F_v) are shown respectively with red and green lines. The force caused by the van der Waals interactions between inner and outer nanotube (F_{vdW}) is represented with a solid blue line.

After roughly $t = 13.8\,\mathrm{ps}$, the inner nanotube expulsion completes and thus F_{vdW} drops to zero. As reported in Fig. 2, this corresponds to the beginning of phase 3, where the inner CNT progressively decelerates because of F_v. It is interesting to observe the similar trend of F_v in Fig. 5(b) with the inner nanotube velocity shown in Fig. 2: this proportionality recalls the viscous damping of a object moving through a fluid [45]. In this view, we model the overall viscous forces as $F_v = -c\dot{x}$, where c is a viscous coefficient and $\dot{x}$ the velocity of the inner CNT.

To estimate the value of the viscous term c, we first analyse the CNT dynamics during the third phase, when only viscous and inertial forces remain. In fact, after the complete nanotube expulsion, the pressure difference between encapsulated and external water vanishes and thus F_i and F_e have no longer effect on the nanotube dynamics, while F_{vdW} tends to zero as well. Therefore, the balance of forces acting on the inner CNT becomes:

$$m\,\ddot{x} + c\,\dot{x} = 0, \tag{4}$$

being m the mass of the nanotube. By solving Eq. 4 and fitting the resulting velocity

8

Table 1. Coefficients of the piecewise-defined function in Eq. 3, which is adopted to interpolate the F_{vdW} values obtained by simulations (blue line in Fig. 5(b)).

a [nN/ps]	b [nN]	d [nN/ps]	e [nN]	f [nN/ps]	g [nN]
14.19	-147.75	0.52	0.50	-32.40	446.62

profile to MD simulations, we obtain a viscous coefficient equal to $1.99 \cdot 10^{-12}$ kg/s. Such value is in reasonable agreement with the literature, for example with the drag coefficient evaluated by Cox and co-authors [46]. Finally, the complete dynamics of the inner CNT during phase 2, 3 and 4 can be described as

$$m\,\ddot{x} + c\,\dot{x} - F_{vdW} + \Delta F_p = 0, \qquad (5)$$

where $\Delta F_p = F_i - F_e$ is the difference between the internal (F_i) and external (F_e) water pressure forces represented in the body diagram in Fig. 5(a).

For instance, Fig. 6 demonstrates an excellent agreement between simulated and predicted (Eq. 5) velocity of the inner nanotube during stage 2, 3, and 4 for the nanorocket setup made of (5,5)(8,8) DWCNT at $T_{heat} = 1600\,$K. Furthermore, Eq. 5 is found to accurately match simulation results also in case of nanorockets based on different DWCNT geometries, e.g. the (8,8)/(11,11) DWCNT setup reported in Appendix A. In these two cases, the dynamical model in Eq. 5 has good prediction capabilities of the inner nanotube motion and, thus, it can be potentially used to predict the nanorocket dynamics in a broad variety of DWCNT configurations once the values of F_{vdW} and ΔF_p are provided.
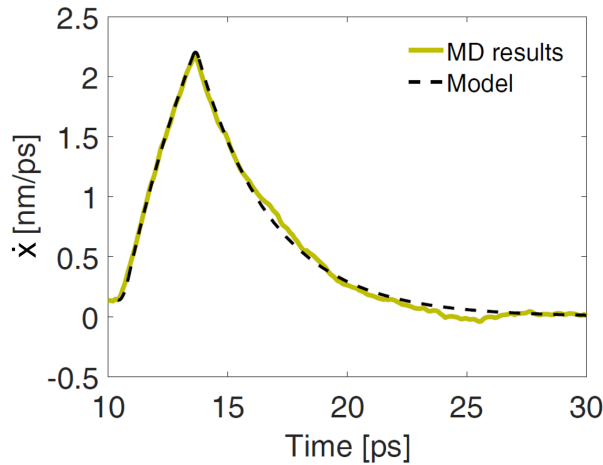

Figure 6. Comparison between simulated and modelled velocity of the inner nanotube during stage 2, 3, and 4 ($T_{heat} = 1600\,$K , (5,5)(8,8) DWCNT setup). The solid yellow line is the velocity of the inner CNT obtained from MD simulations; whereas, the dashed black line represents the velocity transient predicted by Eq. (5).

Notice that, Kapitza resistance is typically high between hydrophobic carbon materials (e.g. carbon nanotubes) and polar solvents (e.g. water), due to their different vibrational properties [47–50]. Therefore, in the simulated nanorocket setup, the Kapitza resistance at the interface between outer carbon nanotube and encapsulated water has a beneficial effect, since it slows down heat dissipation towards surrounding water molecules.

5. Conclusion

In this work, we have proposed and investigated the possibility to use double-walled carbon nanotubes as nanorockets. Using molecular dynamics simulations, we have first studied a test case made of (5,5)/(8,8) DWCNT. Rising the temperature of water molecules encapsulated within the DWCNT, sudden expulsion of the internal nanotube can be triggered. Different temperatures have been analysed and, based on simulation results, we have identified four successive phases of CNT dynamics: a first phase corresponding to the trigger of internal nanotube motion; a second phase regarding the nanotube expulsion; a third phase characterised by the damped motion of the expelled CNT through external water; a fourth phase when final equilibrium conditions are reached.

The forces involved in the inner nanotube dynamics have been analysed in detail, showing that the motion is mainly governed by: first, the pressure force of encapsulated (hot) water; second, the van der Waals interactions between inner and outer nanotube; third, the viscous forces due to external water molecules. Specifically, we have demonstrated that the temperature of encapsulated water regulates the duration of the trigger phase. After this phase, the forces due to encapsulated water become negligible and, therefore, CNT dynamics are mostly controlled by van der Waals interactions and viscous phenomena. In particular, the former are responsible for the expulsion of the inner nanotube, while the latter damp CNT motion through external water. On this basis, we have proposed two models able to predict both the triggering time of CNT expulsion as function of encapsulated water temperature (stage 1), and the inner nanotube dynamics during stage 2, 3, and 4. These models have been shown to accurately recover simulation data. The validity of such dynamical model has been demonstrated also for a different DWCNT configuration, once the different forces acting on the inner nanotube are provided.

The remarkable velocities obtained during the expulsion phase suggest various possible applications of the DWCNT-based nanorockets. As an example, we may think about biomedical applications, such as temperature triggered drug delivery [51,52] and cell membrane piercing [53,54], or engineering ones, such as colloidal suspensions with thermophoretic properties [55,56]. In practical applications, plasmonic or superparamagnetic nanoparticles could be introduced within the DWCNT in order to heat up the encapsulated water, thanks to near-infrared laser or alternating magnetic field exposure, respectively [33,57]. The use of nanotubes with different dimensions would also allow to tune the hollow volume available for the encapsulated water and the inter-layer distance between the nanotubes (and thus van der Waals interactions between them), with the possibility to create configurations in which the inner nanotube motion could be made reversible.

Acknowledgements

Disclosure statement

The authors declare that they have no competing interests.

Appendix A. Configuration made of (8,8)(11,11) DWCNT

To test the validity of the dynamical model in case of different nanorocket configurations, let us consider a second setup characterized by a (8,8)/(11,11) Double-Walled Carbon Nanotube (DWCNT). In this case, the inner (8,8) nanotube has 1.09 nm diameter and 5.24 nm length; whereas, the outer (11,11) nanotube has 1.49 nm diameter and 8.27 nm length. The distance between the open ends of nanotubes is equal to 0.99 nm (see Fig. A1), and the number of encapsulated water molecules is 39.
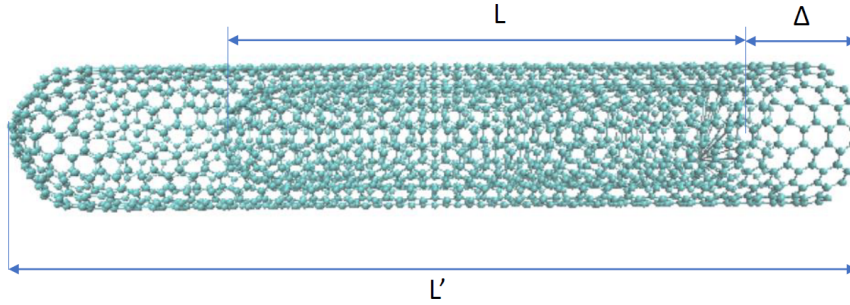

Figure A1. Snapshot of the nanorocket based on (8,8)/(11,11) DWCNT. Water molecules are not represented for clarity.

The behaviour of the (8,8)/(11,11) DWCNT as thermally-driven nanoactuator is studied following the same simulation protocol adopted for the (5,5)/(8,8) DWCNT one. To generalize results, we have analysed the dynamics of inner nanotube expulsion for encapsulated water at $T_{heat} = 2200$ K. Figure A2 reports the forces acting on the inner nanotube during the simulation: the force due to encapsulated water pressure (F_i), the viscous force exerted by external water on the nanotube (F_v), and the interaction force caused by van der Waals interactions between inner and outer nanotube (F_{vdW}) are shown by red, green, and blue lines, respectively.

Although the nature of involved forces remains unchanged between the (8,8)/(11,11) DWCNT (Fig. A2) and (5,5)/(8,8) DWCNT (Fig. 5) configurations, the dynamical behaviour of the two nanoactuators varies, because of the different geometrical parameters and temperature of encapsulated water. Specifically, in case of (8,8)/(11,11) DWCNT, the dynamics of inner nanotube is smoother and the expulsion occurs gradually during the first 20 ps. In fact, Fig. A2 highlights that the motion of the inner nanotube is now characterized by only two distinct phases: the former, occurring during the first 20 ps,

describes the nanotube expulsion due to both internal (F_i) and van der Waals forces (F_{vdW}); the latter, instead, is predominated by viscous damping (F_v).
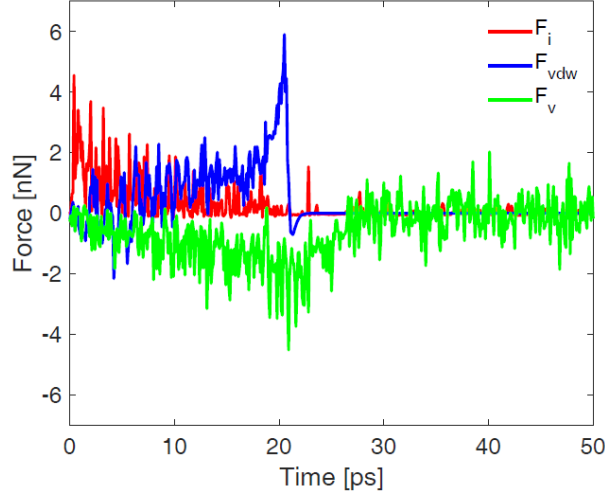

Figure A2. Forces acting on the inner nanotube during the simulation of (8,8)/(11,11) DWCNT configuration. See Fig. 5(a) for the free body diagram of the inner nanotube. Forces are considered as positive if concordant with the expulsion direction.

Considering the whole simulation, namely from $t = 0$ to $50\,\mathrm{ps}$, the van der Waals and internal forces acting on the inner nanotube can be approximated as:

$$F_{vdW} = \begin{cases} \frac{a \cdot t + b}{1 + \exp\left[-c \cdot (t+d)\right]} + f \cdot \exp\left(g \cdot t\right), & \text{if } 0\,\mathrm{ps} < t \le 20.5\,\mathrm{ps} \\ h \cdot t + l, & \text{if } 20.5\,\mathrm{ps} < t \le 21.1\,\mathrm{ps} \\ \frac{m \cdot t + n}{t^2 + p \cdot t + q}, & \text{if } t > 21.1\,\mathrm{ps} \end{cases} \tag{A1}$$

$$F_i = r \cdot \exp\left(-s \cdot t\right). \tag{A2}$$

The parameters of Eqs. A1 and A2 best fitted onto molecular dynamics results (see the yellow lines in Fig. A3) are the following: $a = 0.05$ nN/ps; $b = 0.5$ nN; $c = 8.0$ ps^{-1}; $d = -6.0$ ps; $f = 1.2 \cdot 10^{-11}$ nN; $g = 1.3$ ps^{-1}; $h = -10.8$ nN/ps; $l = 5.9$ nN; $m = 0.04$ nN^2/ps; $n = -1.0$ nN^2; $p = -42.6$ nN/ps; $q = 453.7$ nN; $r = 1.5$ nN; $s = 0.13$ ps.

The complete dynamics of inner nanotube motion can be again described by Eq. 5, where $c = 4.1 \cdot 10^{-12}$ kg/s is now the viscous coefficient obtained from the viscous forces in Fig. A2, and ΔF_p is the difference between the internal (F_i) and external (F_e) water pressure forces. Coherently with the larger diameter of the (8,8) inner nanotube and thus the expected higher hydrodynamic drag, the fitted c value is higher than the one previously found for the (5,5) nanotube. Note that, because of the large temperature difference between encapsulated ($1000 - 2200\,\mathrm{K}$) and external ($300\,\mathrm{K}$) water molecules in the simulated nanorocket configurations, F_e shows negligible values with respect to F_i ones. Finally, Fig. A4 demonstrates an excellent agreement between the simulated
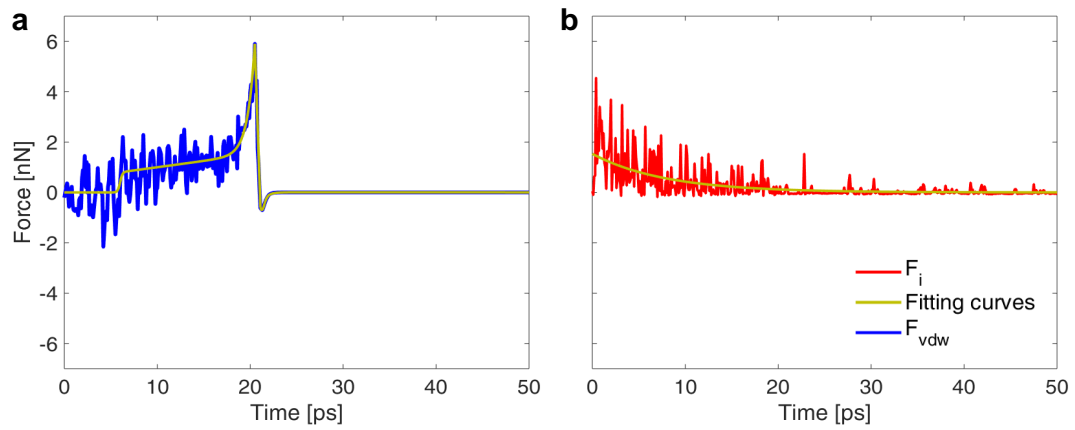
12

Figure A3. (a) Trend of van der Waals forces (F_{vdW}) between inner and outer nanotube in a (8,8)/(11,11) double-walled configuration during the nanorocket dynamics. Molecular dynamics results are depicted in blue; whereas, the yellow line shows the best fitted curve of simulation results (see Eq. A1). (b) Internal forces (F_i) acting on the inner nanotube due to encapsulated water molecules: both simulation results (red line) and fitting curve (yellow line, see Eq. A2) are reported.

and predicted (Eq. 5) velocity of the inner nanotube in the (8,8)/(11,11) DWCNT configuration as well.
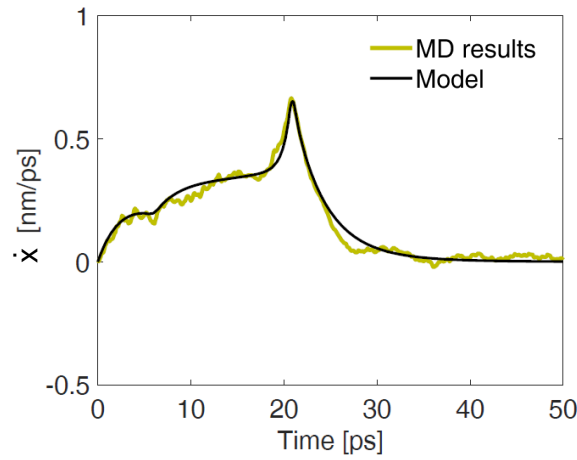

Figure A4. Comparison between simulated (Molecular Dynamics - MD, yellow line) and modelled (Eq. 5, black line) velocity of the inner nanotube in a (8,8)/(11,11) DWCNT nanorocket configuration ($T_{heat} = 2200\,\mathrm{K}$).

References

[1] Wang J. Nanomachines: Fundamentals and applications. 1st ed. Wiley-VCH; 2013.

[2] Gao W, Wang J. The environmental impact of micro/nanomachines: A review. ACS Nano. 2014;8(4):3170–3180.

13

[3] Mavroidis C, Dubey A, Yarmush M. Molecular machines. Annual Review of Biomedical Engineering. 2004;6:363–395.

[4] Kang J, Kwon O, Lee J, et al. Molecular dynamics study of carbon nanotube oscillator on gold surface. Molecular Simulation. 2006;32(5):363–368.

[5] Ozin GA, Manners I, Fournier-Bidoz S, et al. Dream nanomachines. Advanced Materials. 2005;17(24):3011–3018.

[6] Wang J, Manesh KM. Motion control at the nanoscale. Small. 2010;6(3):338–345.

[7] Li J, Rozen I, Wang J. Rocket science at the nanoscale. ACS Nano. 2016;10(6):5619–5634.

[8] Credi A, Venturi M. Molecular machines operated by light. Central European Journal of Chemistry. 2008;6(3):325–339.

[9] Cumings J, Zettl A. Low-friction nanoscale linear bearing realized from multiwall carbon nanotubes. Science. 2000;289(5479):602–604.

[10] Zheng Q, Jiang Q. Multiwalled carbon nanotubes as gigahertz oscillators. Phys Rev Lett. 2002;88:045503.

[11] Legoas SB, Coluci VR, Braga SF, et al. Molecular-dynamics simulations of carbon nanotubes as gigahertz oscillators. Physical review letters. 2003;90(5):055504.

[12] Dong L, Nelson BJ, Fukuda T, et al. Towards nanotube linear servomotors. Automation Science and Engineering, IEEE Transactions on. 2006;3(3):228–235.

[13] Somada H, Hirahara K, Akita S, et al. A molecular linear motor consisting of carbon nanotubes. Nano letters. 2008;9(1):62–65.

[14] Kang JW, Jiang Q, Hwang HJ. A double-walled carbon nanotube oscillator encapsulating a copper nanowire. Nanotechnology. 2006;17(21):5485.

[15] Yuan X, Wang Y. Atomistic simulations on interwall sliding behaviour of double-walled carbon nanotube: effects of structural defects. Molecular Simulation. 2017;43(12):953–961.

[16] Ueno Y, Somada H, Hirahara K, et al. Molecular dynamics simulations for molecular linear motor inside nanotube. Japanese Journal of Applied Physics. 2009;48(6S):06FG03.

[17] Zambrano HA, Walther JH, Jaffe RL. Thermally driven molecular linear motors: a molecular dynamics study. The Journal of chemical physics. 2009;131(24):241104.

[18] Guo W, Gao H. Optimized bearing and interlayer friction in multiwalled carbon nanotubes. Comput Model Eng Sci. 2005;7(1):19–34.

[19] Kang JW, Song KO, Kwon OK, et al. Carbon nanotube oscillator operated by thermal expansion of encapsulated gases. Nanotechnology. 2005;16(11):2670.

[20] Xia Z, Curtin WA. Pullout forces and friction in multiwall carbon nanotubes. Physical Review B. 2004;69(23):233408.

[21] Li Y, Hu N, Yamamoto G, et al. Molecular mechanics simulation of the sliding behavior between nested walls in a multi-walled carbon nanotube. Carbon. 2010;48(10):2934–2940.

[22] Yamamoto G, Liu S, Hu N, et al. Prediction of pull-out force of multi-walled carbon nanotube (mwcnt) in sword-in-sheath mode. Computational Materials Science. 2012;60:7–12.

[23] Liu P, Zhang Y. Translational dynamic friction analysis of double-walled carbon nanotubes. Molecular Simulation. 2011;37(2):84–89.

[24] Hess B, Kutzner C, Van Der Spoel D, et al. Gromacs 4: algorithms for highly efficient, load-balanced, and scalable molecular simulation. Journal of chemical theory and computation. 2008;4(3):435–447.

[25] Kumar H, Dasgupta C, Maiti PK. Driving force of water entry into hydrophobic channels of carbon nanotubes: entropy or energy? Molecular Simulation. 2015;41(5-6):504–511.

[26] Chiavazzo E, Fasano M, Asinari P, et al. Scaling behaviour for the water transport in nanoconfined geometries. Nature communications. 2014;5.

[27] Fasano M, Chiavazzo E, Asinari P. Water transport control in carbon nanotube arrays. Nanoscale research letters. 2014;9(1):559.

[28] Robinson M, Marks N. Nanocap: A framework for generating capped carbon nanotubes and fullerenes. Computer Physics Communications. 2014;185(10):2519–2526.

[29] Berendsen HJC, Grigera JR, Straatsma TP. The missing term in effective pair potentials. Journal of Physical Chemistry. 1987;91(24):6269–6271.

14

[30] Nosé S, Klein ML. Constant pressure molecular dynamics for molecular systems. Molecular Physics. 1983;50(5):1055–1076.

[31] Parrinello M, Rahman A. Polymorphic transitions in single crystals: A new molecular dynamics method. Journal of Applied physics. 1981;52(12):7182–7190.

[32] Amendola V, Pilot R, Frasconi M, et al. Surface plasmon resonance in gold nanoparticles: a review. Journal of Physics: Condensed Matter. 2017;29(20):203002.

[33] Gizzatov A, Key J, Aryal S, et al. Hierarchically structured magnetic nanoconstructs with enhanced relaxivity and cooperative tumor accumulation. Advanced functional materials. 2014;24(29):4584–4594.

[34] Harris N, Ford MJ, Cortie MB. Optimization of plasmonic heating by gold nanospheres and nanoshells. The Journal of Physical Chemistry B. 2006;110(22):10701–10707.

[35] Boriskina SV, Ghasemi H, Chen G. Plasmonic materials for energy: From physics to applications. Materials Today. 2013;16(10):375–386.

[36] Setoura K, Okada Y, Hashimoto S. Cw-laser-induced morphological changes of a single gold nanoparticle on glass: observation of surface evaporation. Physical Chemistry Chemical Physics. 2014;16(48):26938–26945.

[37] Carlson MT, Khan A, Richardson HH. Local temperature determination of optically excited nanoparticles and nanodots. Nano letters. 2011;11(3):1061–1069.

[38] Bergamasco L, Alberghini M, Fasano M, et al. Mesoscopic moment equations for heat conduction: Characteristic features and slow–fast mode decomposition. Entropy. 2018; 20(2):126.

[39] Hockney R, Goel S, Eastwood J. Quiet high-resolution computer models of a plasma. Journal of Computational Physics. 1974;14(2):148–158.

[40] Reißer S, Poger D, Stroet M, et al. Real cost of speed: the effect of a time-saving multiple-time-stepping algorithm on the accuracy of molecular dynamics simulations. Journal of chemical theory and computation. 2017;13(6):2367–2372.

[41] Miyamoto S, Kollman PA. Settle: An analytical version of the shake and rattle algorithm for rigid water models. Journal of computational chemistry. 1992;13(8):952–962.

[42] Crisafulli A, Khodayari A, Mohammadnejad S, et al. Sliding dynamics of parallel graphene sheets: Effect of geometry and van der waals interactions on nano-spring behavior. Crystals. 2018;8(4):149.

[43] Karim MR, Li X, Kang P, et al. Ultrafast pulsed laser induced nanocrystal transformation in colloidal plasmonic vesicles. Advanced Optical Materials. 2018;:1800726.

[44] Keller EL, Frontiera RR. Ultrafast nanoscale raman thermometry proves heating is not a primary mechanism for plasmon-driven photocatalysis. ACS nano. 2018;12(6):5848–5855.

[45] Morciano M, Fasano M, Nold A, et al. Nonequilibrium molecular dynamics simulations of nanoconfined fluids at solid-liquid interfaces. The Journal of chemical physics. 2017; 146(24):244507.

[46] Cox R. The motion of long slender bodies in a viscous fluid part 1. general theory. Journal of Fluid mechanics. 1970;44(4):791–810.

[47] Tascini AS, Armstrong J, Chiavazzo E, et al. Thermal transport across nanoparticle–fluid interfaces: the interplay of interfacial curvature and nanoparticle–fluid interactions. Physical Chemistry Chemical Physics. 2017;19(4):3244–3253.

[48] Konatham D, Papavassiliou D, Striolo A. Thermal boundary resistance at the graphene–graphene interface estimated by molecular dynamics simulations. Chemical Physics Letters. 2012;527:47–50.

[49] Wang Y, Keblinski P. Role of wetting and nanoscale roughness on thermal conductance at liquid-solid interface. Applied Physics Letters. 2011;99(7):073112.

[50] Alexeev D, Chen J, Walther JH, et al. Kapitza resistance between few-layer graphene and water: liquid layering effects. Nano letters. 2015;15(9):5744–5749.

[51] Chen X, Chen H, Tripisciano C, et al. Carbon-nanotube-based stimuli-responsive controlled-release system. Chemistry-A European Journal. 2011;17(16):4454–4459.

[52] Qin Y, Chen J, Bi Y, et al. Near-infrared light remote-controlled intracellular anti-cancer drug delivery using thermo/ph sensitive nanovehicle. Acta biomaterialia. 2015;17:201–209.

[53] Lacerda L, Ali-Boucetta H, Kraszewski S, et al. How do functionalized carbon nanotubes land on, bind to and pierce through model and plasma membranes. Nanoscale. 2013; 5(21):10242–10250.

[54] Rochal SB, Roshal DS, Myasnikova AE, et al. Commensurability between protein nanotubes in contractile ejection nanomachines. Nanoscale. 2018;.

[55] Cardellini A, Fasano M, Bigdeli MB, et al. Thermal transport phenomena in nanoparticle suspensions. Journal of Physics: Condensed Matter. 2016;28(48):483003.

[56] Fasano M, Bigdeli MB. Bottom up approach toward prediction of effective thermophysical properties of carbon-based nanofluids. Heat Transfer Engineering. 2017;:1–12.

[57] Guerrero AR, Hassan N, Escobar CA, et al. Gold nanoparticles for photothermally controlled drug release. Nanomedicine. 2014;9(13):2023–2039.